Deterministic Optimization of Single-Slotted Flaps Using an Automated CFD Workflow

Mara-Florina NEGOITA*[1,2], Alina BOGOI[2], Ionut BUNESCU[1,2], Mihai-Vladut HOTHAZIE[1,2]

*Corresponding author
[1]INCAS – National Institute for Aerospace Research "Elie Carafoli",
B-dul Iuliu Maniu 220, Bucharest 061126, Romania,
negoita.mara@incas.ro*, bunescu.ionut@incas.ro, hothazie.mihai@incas.ro
[2]Department of Aerospace Sciences,
National University of Science and Technology POLITEHNICA Bucharest,
Gheorghe Polizu 1, 011061, Bucharest, Romania,
alina.bogoi@upb.ro

DOI: 10.13111/2066-8201.2025.17.4.8

Received: 19 September 2025/ Accepted: 10 November 2025/ Published: December 2025

Abstract: *While aerodynamic optimization of wing geometry in cruise flight has been widely investigated, such modifications inevitably alter the aerodynamic characteristics of high-lift devices, which remain essential during take-off and landing regimes. In this context, the present study addresses the influence of flap slot geometry on the aerodynamic characteristics of single-slotted flap configurations. For this reason, a parametrization method is introduced, combining cubic Bézier curves for flap definition with local curvature parameters for the cove region of the airfoil. This approach ensures geometric continuity in the retracted configuration while enabling rigorous control of the deployed flap geometry. The parametrization was integrated into an automated CFD and gradient-based optimization framework, enabling the efficient exploration of six geometric parameters across multiple configurations. The analysis revealed that lip length and the curvature of the flap's upper surface have the most significant impact on aerodynamic performance, influencing lift generation, flow attachment, and drag reduction. Optimized configurations achieved up to a 7% increase in maximum lift coefficient and a 5% reduction in drag relative to the baseline geometry. These results highlight the potential of precise geometric control of flap slots to enhance aerodynamic efficiency, particularly in low-speed regimes relevant to take-off and landing. The proposed methodology establishes a foundation for advanced parametrization and optimization strategies for multi-element airfoil configurations and next-generation high-lift systems.*

Key Words: *deterministic optimization, single-slotted flap, CFD, parametrization, Bézier curves*

1. INTRODUCTION

Fuel consumption reduction in general and commercial aviation alike has become a crucial objective, along with the European Union intention of completely eliminating carbon emissions by 2050 [1]. Consequently, a frequent approach lies in the geometrical optimization of airfoil and wing configurations in cruise flight, in order to reduce the needed fuel consumption [2]. Still, wing geometry optimization inevitably alters the aerodynamic

characteristics when high-lift devices are deployed. Consequently, an additional process of optimization and validation is essential for ensuring that the aerodynamic performance meets the necessary requirements not only in cruise, but also during take-off and landing [3].

During critical flight regimes, the deployment of the flap is essential for generating additional lift and reducing the runway length for safe take-off and landing, as proven by various approaches, such as the reference study performed by A.M.O. Smith [4], along with numerical methods by J. Bodart in [5] and B. Steenwijk in [6], as well as extended experimental campaigns, whose results are presented in [6]. The increased geometrical complexity of single-slotted flaps generates several phenomena, such as flow separation and turbulent boundary layers, behaviors inherently dependent on the internal geometry of the slot [7]. The investigation of flap's slot influence, defined as the region between the main airfoil and the leading edge of the deployed flap, requires rigorous control of the geometrical definition. Thus, a parametrization method is required. Although multiple parametrization methods are frequently used for mapping airfoils based on a series of design variables, such as the NACA 4,5,6 digits series [referents], Class Shape Transformation [8], PARSEC [9] no widely acknowledged parametrization techniques exist for multi-element configurations. Flap geometry parametrization is particularly challenging, as the primary constraint is to preserve the retracted configuration unmodified, in order to maintain surface continuity and curvature alignment. This condition ensures that the aerodynamic characteristics in cruise remain unaffected by geometric modifications of the flap.

In his 2011 study, G.D. Howe [11] used a fourth order Bézier curve for defining the leading edge, while keeping the rest of the flap unmodified. This approach has proved itself useful in controlling the aspect of the slot but failed in capturing the influence of lip length and the cove trailing edge point, located on the main airfoil, as it was designed solely by imposing a gap between the airfoil and flap, therefore ignoring practical and technological practices and aerodynamic characteristics. Furthermore, his method offered no control over the location point of the flap leading edge.

Consequently, the present study builds on the idea of using Bézier curves to provide geometric definition of the flap, while introducing an additional parametrization for the cove region of the airfoil and changing the fourth order curve with two conjoint third order, for rigorously designing the leading edge location.

Optimization of multi-element configurations have been performed by multiple authors, such as [12] and [13], who focused on blown flaps, as well as W. Chen et al., whose integration of Generative Adversarial Networks substantially reduced the computational effort associated with the process [14], whereas in [11], a deterministic and a stochastic optimization method have been compared, with the deterministic offering more accurate estimations. The optimization of a single-slotted flaps using a deterministic method was considered suitable for the present study, due to its lower computational effort compared to stochastic methods, which results from the reduced number of iterations required for convergence, as well as its high reproducibility and directional space exploration capability.

2. METHODOLOGY

A. Parametrization Method

The initial configuration is based on the NACA 23012 airfoil [4, 15], modified to include both the flap and the slot. The developed technique maps the internal region of the configuration, represented by the inner slot of the airfoil, parametrized with respect to the local curvatures of

the slot, along with the leading edge flap, by using a modified Bézier parametrization, highlighted in red in Fig. 1.

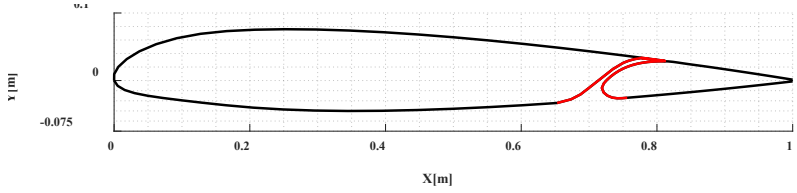

Fig. 1. NACA 23012 airfoil designed with a single slotted flap at $0.72c$

Bézier curves are widely employed for airfoil geometry representation, using four curves defined through polynomial functions of the form [11], as presented in (1):

$$P(t) = \sum_{k=0}^{m} C_m^k \, t^k (1-t)^{m-k} P_k \tag{1}$$

where $C_m^k = \frac{m!}{k!(m-k)!}$ represents the binomial coefficient, for $n \geq 2$, a parameter $t \in [0,1]$ and a series of $m+1$ control points $P_0, P_1 \ldots, P_m$.

An airfoil definition typically requires 13 control points. In the case of the flap leading edge, the upper and lower surface curves extending from the trailing edge were fixed. Enforcing continuity at the leading-edge point further constrained the design space, reducing the parametrization to only three effective design variables in the region of interest. Fig. 2 offers a visual representation of the control points mapping the curvature location and aspect of the leading edge.

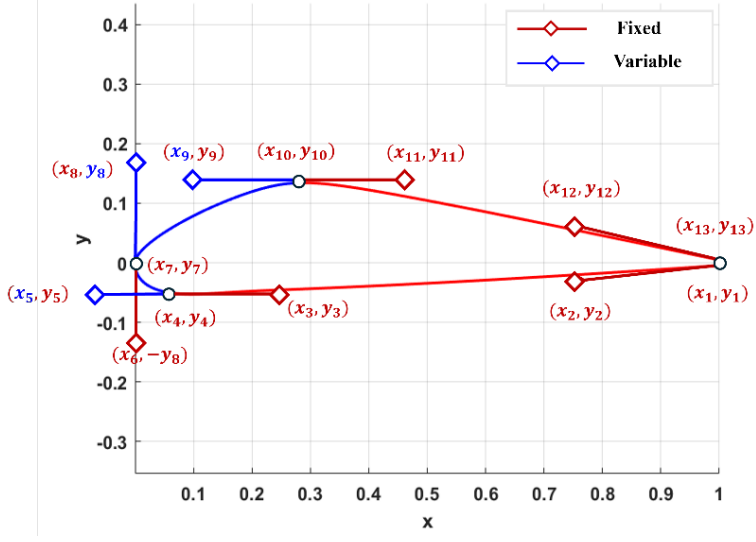

Fig. 2 Display of Bézier control points used for the parametrization method

Parametrization of the inner slot region was achieved by means of two circular arcs of radii R_1, tangent to the unmodified geometry of the lower surface, and R_2, tangent to the slot lip. The third variable is represented by L, the lip length, whereas its thickness was imposed by technological, manufacturing constraints.

The three imposed parameters, alongside the highlighted point P, marking the given geometry of the lower surface, are represented in Fig. 3.

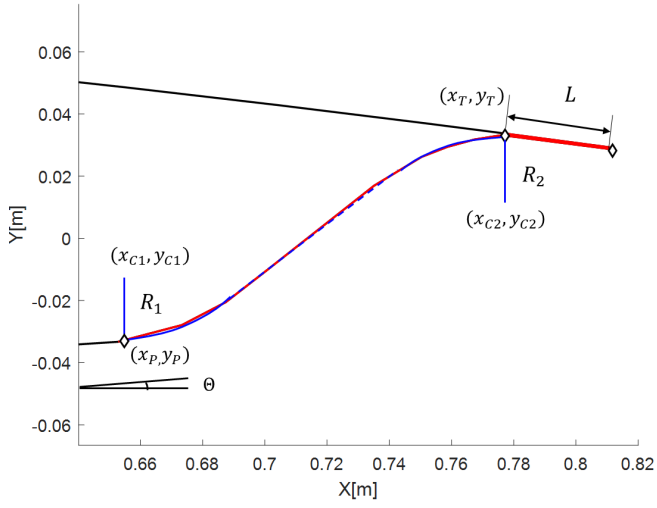

Fig. 3 Inner slot parametrization

The position of the two circle centers C_1 and C_2 were determined by using the circle equation, with respect to the position of the fixed point P, as well as θ, representing the inclination of the lower surface. So, the position of center C_1 is mathematically expressed as:

$$\begin{aligned} x_{c_1} &= x_P - R_1 \cos\left(3\frac{\pi}{2} + \theta\right) \\ y_{c_1} &= y_P - R_1 \sin\left(3\frac{\pi}{2} + \theta\right). \end{aligned} \tag{2}$$

For generating the upper surface lip, starting from the last specified point, an extension is made by the prescribed length L. The direction of the constructed region matches the direction of the vector defined by the last points of the airfoil configuration, and is determined by the following equation:

$$r_{X_n} = r_{X_{n-1}} + \overrightarrow{X_{n-1}X_n} \tag{3}$$

Due to manufacturing constraints, the lip thickness of the slot was maintained at a constant value of:

$$l = 0.001m \tag{4}$$

Similarly, the inner surface of the lip was determined by performing a translation by the trailing edge thickness:

$$y = y_{upper} + l \tag{5}$$

For the inner tangent circle, the center was determined to be identical to that of the circle tangent to the upper circle, based on the radius and the last known point of the preserved geometry:

$$\begin{aligned} x_{c_2} &= x_t - R_2 \cos\left(\frac{\pi}{2} - \theta\right) \\ y_{c_2} &= y_t - R_2 \sin\left(\frac{\pi}{2} - \theta\right). \end{aligned} \tag{6}$$

Considering the of the two tangent circles, the internal tangent to the circles was created using the intermediate circle method.

As presented in Fig. 4 – (a), a third circle was thus generated, with a radius of:

$$R_3 = R_1 + R_2. \tag{7}$$

The distance between the two centers has then been calculated, as seen in Fig. 4 (b):

$$H = \sqrt{(x_2 - x_1)^2 + (y_2 - y_1)^2} \tag{8}$$

with angle φ representing:

$$\varphi = \arcsin\left(\frac{R_3}{H}\right). \tag{9}$$

Depending on the value of angle φ, the point of tangency T_1 to the intermediate circle is identified in Fig. 4 (c).

Subsequently, the line is translated by the radius value R_1, so that the resulting line, T_1T_2, becomes the exact internal tangent to both circles as seen in Fig. 4 (d).

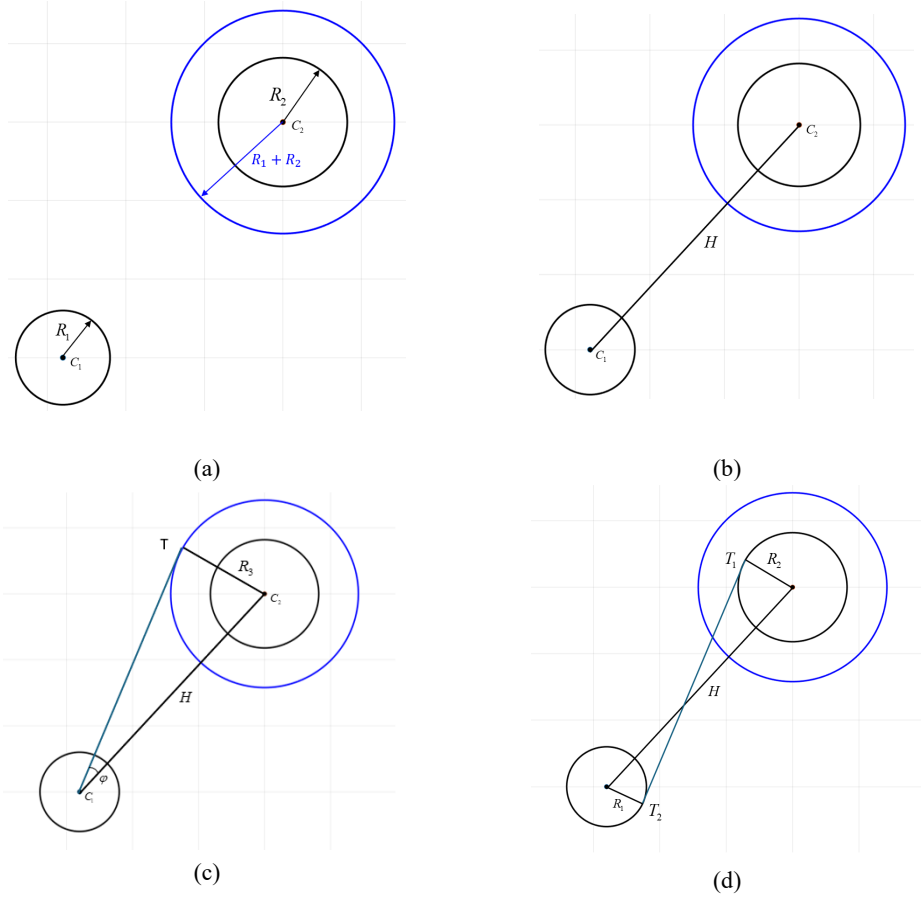

Fig. 4 The algorithm used for constructing the interior tangent to the given circles

The two algorithms employed for the parametrization of the single-slotted flap yields six parameters that define the configuration geometry. These parameters are denoted as W_i, for $i \in [1,6]$, as presented in Fig. 5.

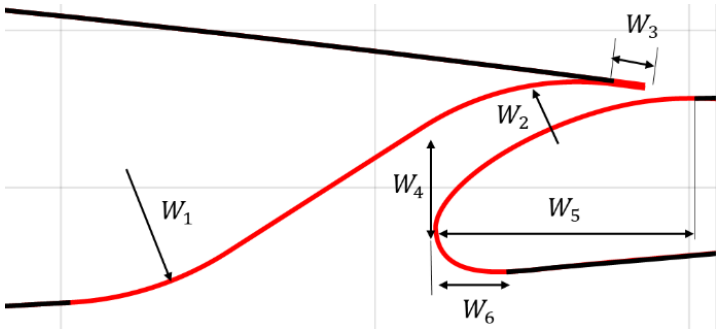

Fig. 5 Visual representation of the 6 design variables

B. Automation Workflow

The developed parametrization was later integrated in a fully-automated CFD workflow, allowing for the continuous generation of computational domains in ANSYS Design Modeler, followed by the export of unstructured meshes using Ansys Meshing and CFD simulations performed by ANSYS Fluent, integrated through a MATLAB script. Subsequently, the automation allowed for efficient design space exploration, elaborated through a parametric study.

The automation workflow was integrated into a MATLAB script, where the geometric parameters, through the parametrization method, generate the airfoil and flap coordinates, which are then exported to a text file. Next, the use of a Window batch file allowed for the automatic replacement of the airfoil geometry into the computational domain using Design Modeler, followed by the mesh generation and export in Ansys Meshing. The commands for generating the domain were transmitted to Design Modeler and Ansys Meshing via a JScript file. Finally, the simulations were performed in Fluent, where the grid import, case initialization, boundary condition setup, and specification of the number of iterations were automated through a text-based journal file. After each simulation, the coefficients of lift and drag were returned, and the process was repeated for a new geometric configuration. A schematic representation of the developed automation workflow is shown in Fig. 6.

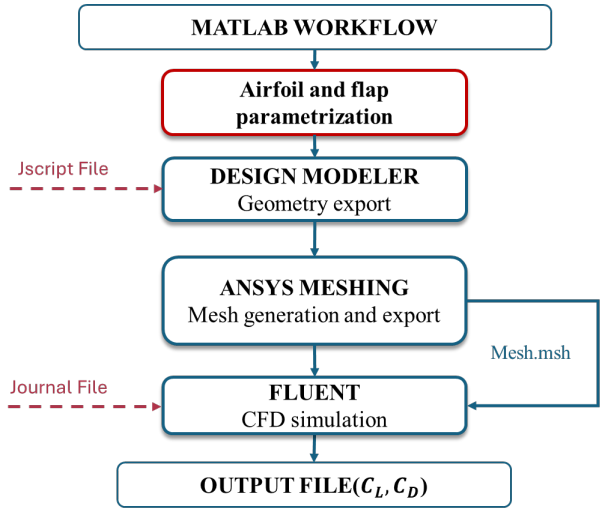

Fig. 6 CFD automation workflow

Around the given geometry, a circular computational domain was created, a choice suitable for the desired analysis, due to reduced interaction between the domain boundaries and the target configuration. A radius of 40 m was selected to ensure sufficient distance between the object and the domain boundary, preventing boundary condition interactions in subsonic regime.

An unstructured mesh was used to facilitate integration into the automation process, consisting of triangular elements in the fluid domain and quadrilateral elements in the boundary layer region near solid surfaces to accurately capture viscous effects and flow separation in the slot region induced by flap deflection. The boundary layer grid was generated with an inflation algorithm, with the first cell height set to achieve $y^+ = 1$, a growth ratio of 1.15, and a total of 60 layers.

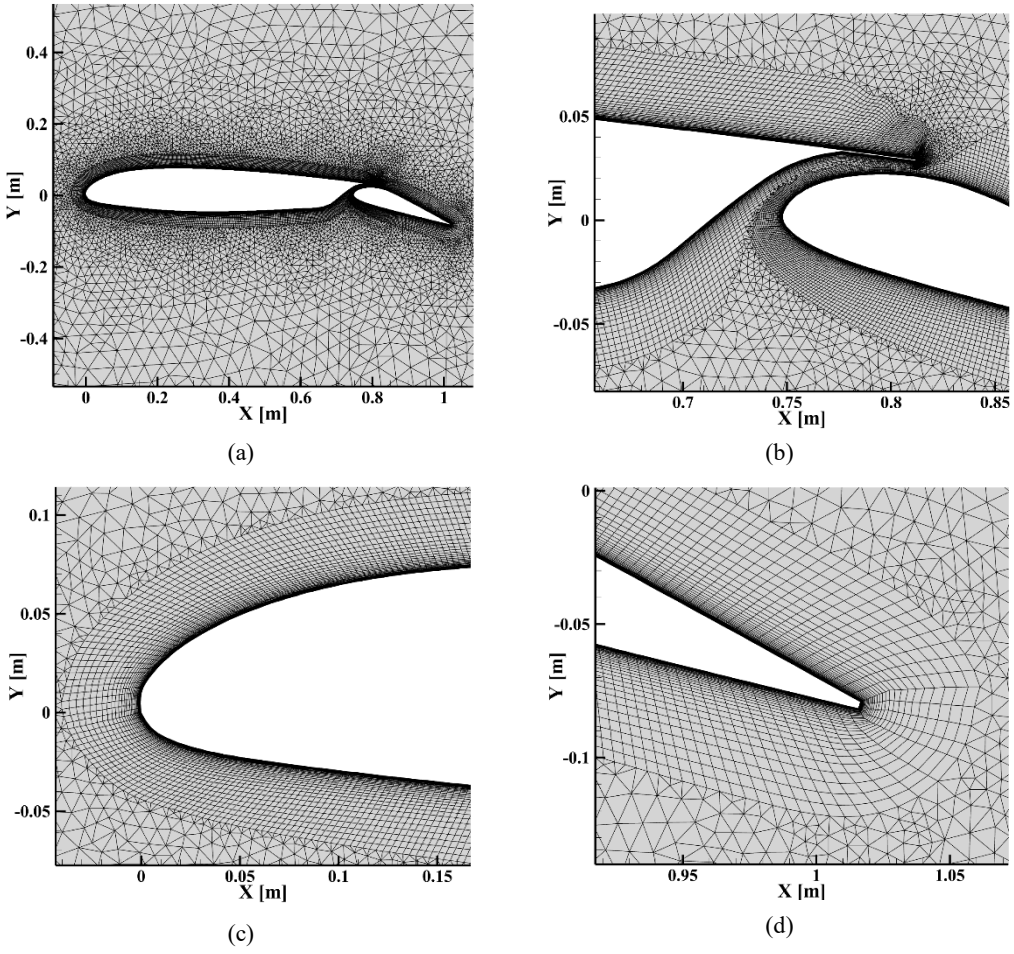

Fig. 7 Mesh around the single-slotted flap

All configurations have been analyzed for a deflection flap angle of 20°, corresponding to the take-off case, as well as a free-stream velocity of 60 m/s. The deflected flap generates strong adverse pressure gradients in the slot region, making the flow prone to boundary-layer separation. At the same time, the converging region of the cove accelerates the flow, leading to high local velocity gradients and increased shear stresses near the wall. For this reason, the $k-\omega$ SST turbulence model was employed, capable of accurately resolving the near-wall region while also maintaining robustness in separated flow regimes.

A grid-independence study was conducted to assess the influence of mesh density on the numerical solutions. Four meshes of increasing number of elements were generated, ranging from coarse to very fine. Simulations were performed for each mesh at several angles of attack to evaluate the sensitivity of the results to the chosen discretization.

In all cases, the first-cell height and the number of inflation layers in the near-wall region were kept constant, while the surface discretization step, maximum element size in the far-field domain, and element growth rate were varied. The resulting meshes contained between 23,000 and 93,000 elements. Obtained coefficients of drag and lift for each of the investigated meshes are presented in Fig. 8.

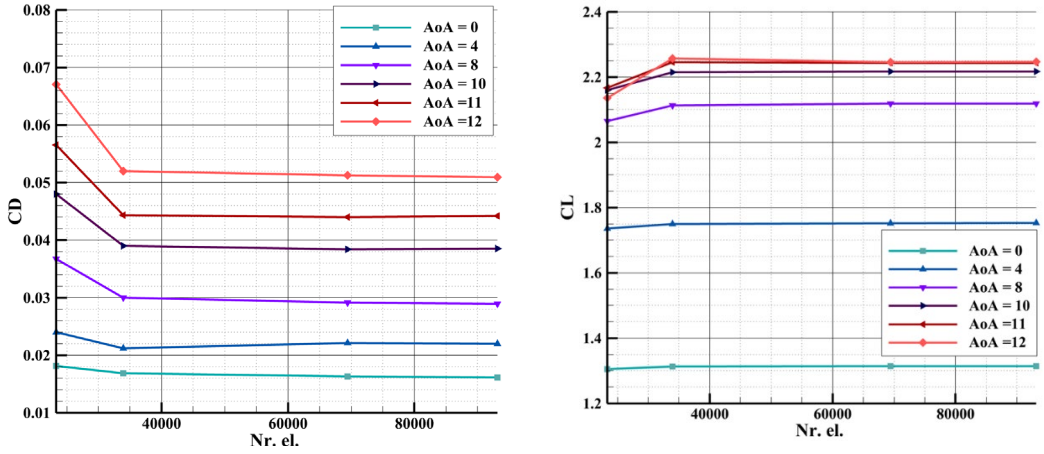

(a) (b)

Fig. 8 Variation of the drag (a) and lift (b) coefficients for different mesh sizes

While substantial variations in the aerodynamic coefficients were observed between the coarse and medium meshes, these differences have been reduced for the finer grids. Compared to the extra-fine mesh, the grid with 69,000 elements produced comparable results, exhibiting proper behaviors with insignificant variations across all angles of attack considered, even in the non-linear, near stall region. Therefore, the use of a fine mesh for the simulations was considered an appropriate compromise between result accuracy and the computational cost associated with a higher-density grid.

C. Parametric Analysis

The developed parametrization method, along with the automation flow, enabled the continuous evaluation of multiple configurations, providing an effective approach for a parametric analysis. The influence of each parameter has been investigated by selecting three representative values, ranging from the lower to the upper feasible limit and generated a database of 729 configurations. Since not all parameter combinations produce feasible configurations, certain constraints have been imposed to ensure possible solutions. If lower bounds have been considered so that the inner slot presents minimal curvature radii and an inner tangent exists, upper limits were imposed by two intersection conditions: one to prevent the intersection of the flap with the main airfoil both in retracted and deflected configurations, and the other dictated by the reasonable size of the inner slot radii.

D. Optimization Process

The objective of the optimization process was to identify the geometry that has superior performance in the take-off configuration. The focus was on enhancing the lift coefficient in

the nonlinear region of the polar curve, particularly the maximum lift coefficient , associated with the stall angle of attack. The chosen algorithm was *fmincon*, integrated within MATLAB, which provides several gradient-based solvers that can be selected depending on the problem characteristics. An unconstrained optimization was carried out, with the upper ($\boldsymbol{UB}$) and lower ($\boldsymbol{LB}$) parameter bounds and the objective function defined as:

$$\min\left(f_{\text{obj}}(\boldsymbol{W})\right) = \frac{1}{C_{L_{max}}}, where\ \boldsymbol{LB} \leq \boldsymbol{W} \leq \boldsymbol{UB} \tag{10}$$

For this study, a deterministic, gradient-based optimization algorithm was selected, offering fast convergence and high reproducibility. Unlike stochastic methods, deterministic approaches allow a targeted exploration of the design space, significantly reducing the number of CFD evaluations required. For further reducing the computational time associated with the optimization process, the previously developed parametrization method was integrated to constitute the design variable exploration, whereas the automation was used for evaluating the objective function. The optimization begins from a reference geometry defined by the selected parameters, using the Sequential Quadratic Programming (SQP) algorithm. Gradients are estimated via first-order finite differences, and the geometry is iteratively updated along the descent direction with an adaptive step size until convergence. The algorithm is schematically illustrated in Fig. 9.

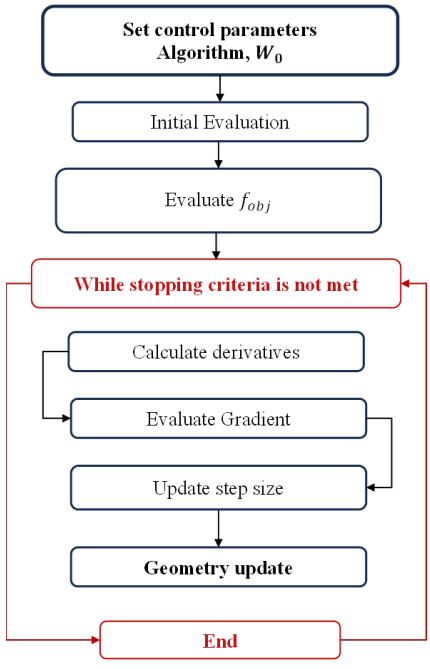

Fig. 9 Gradient optimization flowchart

3. RESULTS

A. Numerical Simulation

Initial CFD simulations have been performed for understanding the impact of the flap deployed during take-off, as well as the influence of the flap slot in cruise, as compared to the plain airfoil. The gap generated by the presence of the slotted flap should, ideally, not modify

the aerodynamic characteristics of the retracted configuration, so that the cruise flight, the one responsible for most of the fuel consumption, is not negatively affected by installed high-lift devices. Fig. 10 shows comparative results between the three evaluated configurations. As compared to the plain NACA23012, the retracted flap geometry presents comparable results in the lift coefficient, at low and moderate angles of attack, indicating no significant influence of the slot. At angles of attack surpassing 10°, the slot effect becomes visible, corresponding to a maximum drop of 6% in lift. Still, differences in the nonlinear region are expected and not of interest for evaluating the cruise region, as such high angles of attack typically require the deployment of high-lift devices. Nevertheless, the drag generated by the retracted geometry shows a quasi-parallel distribution to the NACA23012, with a constant increase close to 5% along the polar curve, due to the added form drag generated by the gap between the airfoil and flap. Flap deployment in take-off configuration presents a significant increase in lift and drag alike, resulting in a shift of the polar, with a maximum increase in lift-to-drag value of 38% as compared to the plain airfoil. The extended camber and chord value positively affect the lift coefficient, while simultaneously increasing drag, due to both additional parasitic and induced drag.

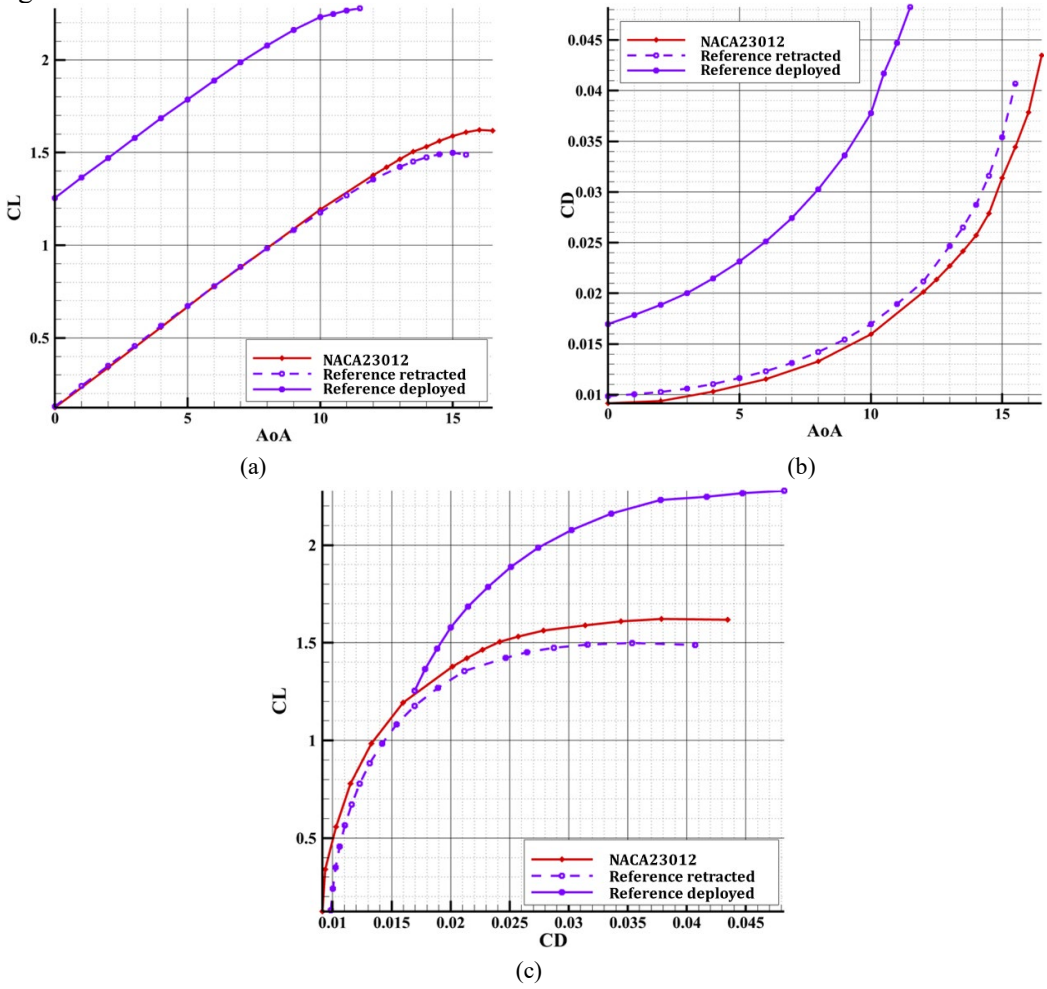

Fig. 10 Comparative variation of aerodynamic characteristics for the plain airfoil, retracted flap and flap deployed at 20°

The influence of the flap and slot are most visible in the velocity contour, alongside the streamline distributions displayed in Fig. 11, where accelerations on the upper surface of the airfoil, as well as separation regions offer significant insight about the influence of the slotted flap. At zero angle of attack, the retracted configuration has a similar velocity distribution as the plain NACA23012, as there is no airflow through the slot, indicating little to no modifications in cruise region.

Nonetheless, in Fig. 11 - (c), the deployment allows for the flow to pass through the slot on the flap, generating a secondary acceleration, therefore resulting in increased velocity magnitude.

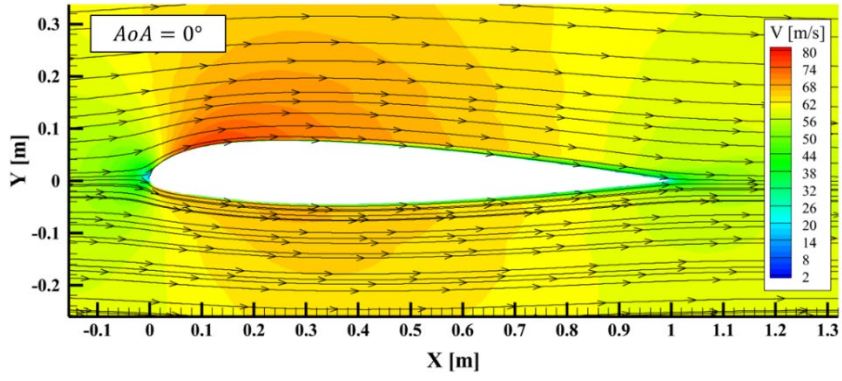

(a)

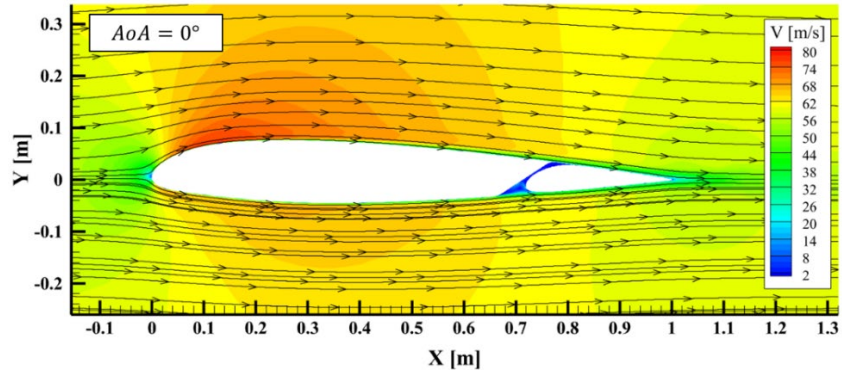

(b)

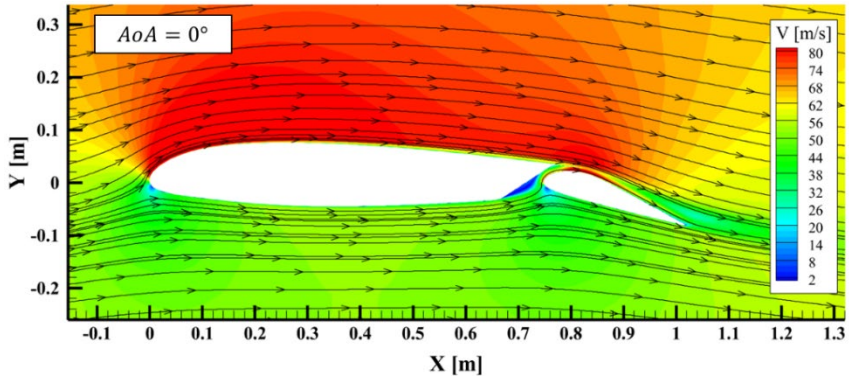

(c)

Fig. 11 Velocity contours for the plain airfoil (a), retracted flap (b) and flap deployed at 20° (c)

B. Parametric Study

Following the individual analysis of feasible combinations of geometric parameters, the influence of each parameter was assessed by keeping five parameters constant while varying only one. Fig. 15 illustrates the variation of lift and drag coefficients with the angle of attack, as a function of a single geometric parameter of the slot.

For parameters W_1 and W_2, corresponding to the two curvature radii of the interior slot region, the results indicate that their influence on both lift and drag is negligible, as presented in Fig. 12. The lift coefficient curves nearly overlap across all tested values, showing no meaningful deviations up to an angle of attack of 13°. Similarly, the drag coefficient presents a consistent trend with only marginal differences between configurations. At lower angles of attack, slight differences appear in the drag coefficient, primarily due to variations in form drag caused by changes in the slot aspect ratio. However, these differences diminish and become insignificant as the angle of attack increases.

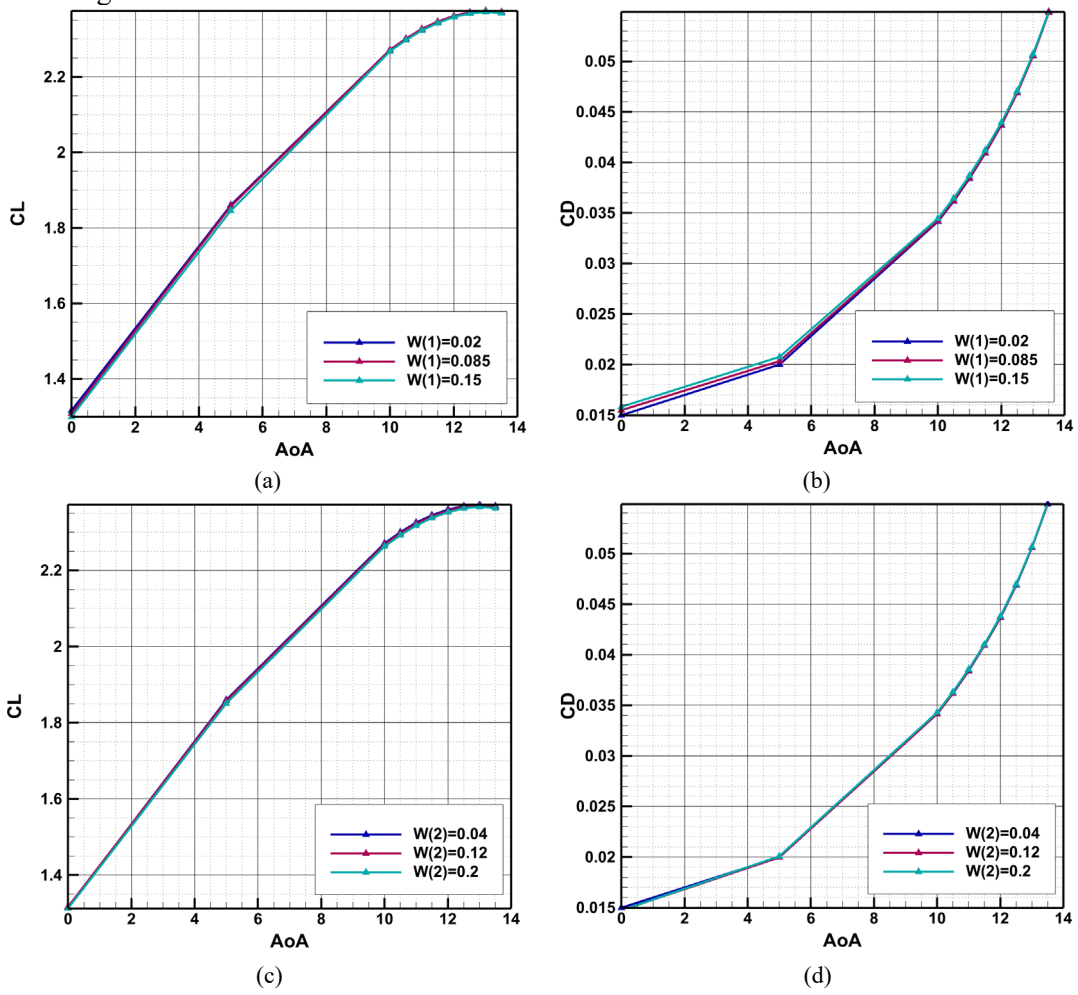

Fig. 12 CL vs AoA and CD vs AoA for different values of W_1(a-b) and W_2 (c-d)

Parameter W_3, corresponding to the lip length exhibits the most noticeable aerodynamic impact. While the trends displayed in Fig. 13 remain similar to those observed for the first two parameters, clear differences emerge as the angle of attack increases. Reduced lip length leads

to higher lift values, particularly in the nonlinear region of the polar curve. This effect arises from the geometry at the slot exit, a region responsible for accelerating the airflow over the flap's upper surface. A shorter lip creates a larger flow area and enhances the energy of the airflow, causing the boundary layer to remain attached. In particular, larger values of W_3 reduce the maximum lift coefficient, with discrepancies becoming significant beyond AoA = 10°.

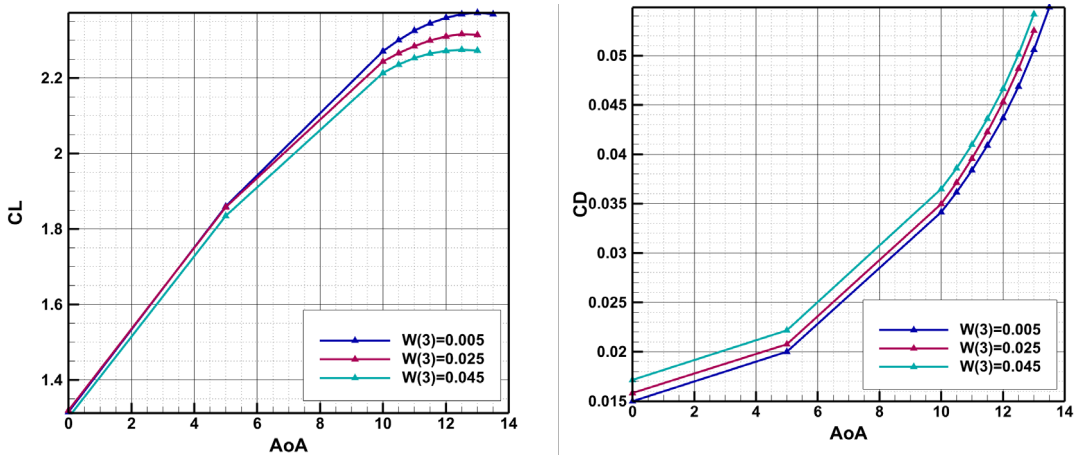

(a) (b)

Fig. 13 $CL\ vs\ AoA$ (a) and $CD\ vs\ AoA$ (b) for different values of W_3

For W_4, the parameter designing the aspect and curvature of the upper surface of the flap, a noticeable sensitivity is observed in both lift and drag characteristics. At low and moderate angles of attack, reduced values exhibit consistently higher lift coefficients, with differences becoming more pronounced in the nonlinear region of the polar. Furthermore, the larger value of the parameter causes premature stall, occurring at $\mathrm{AoA} = 12.5°$, as the increased camber generates enhanced flow separation behind the maximum curvature point, as well as higher drag values.

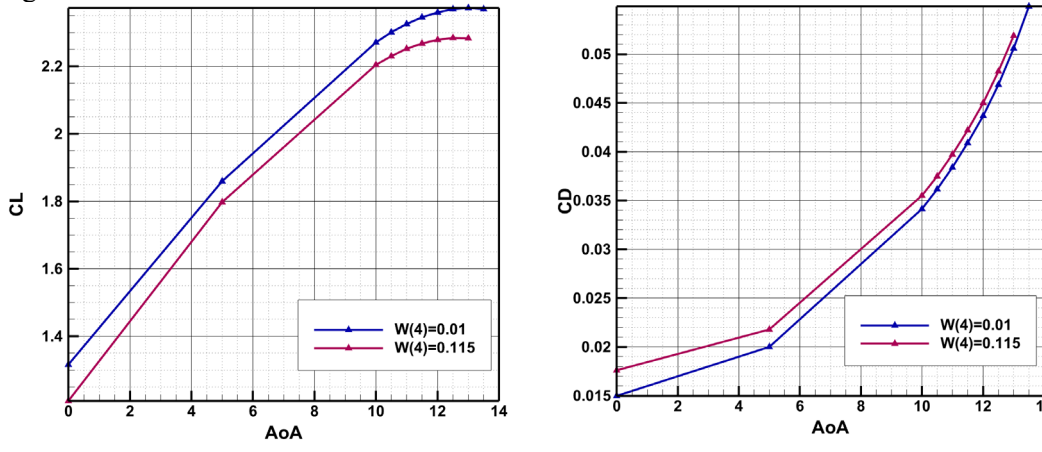

(g) *(h)*

Fig. 14 $CL\ vs\ AoA$ (a) and $CD\ vs\ AoA$ (b) for different values of W_4

As for parameters W_5 and W_6, responsible for the aspect of the flap leading edge and the lower surface, subtle changes in lift coefficients behavior can be observed for angles of attack lower than $\mathrm{AoA} = 10°$, a diminishing effect as the configurations get closer to the stall region.

Similarly, even less pronounced variations, not surpassing 1%, have been observed for the drag coefficient.

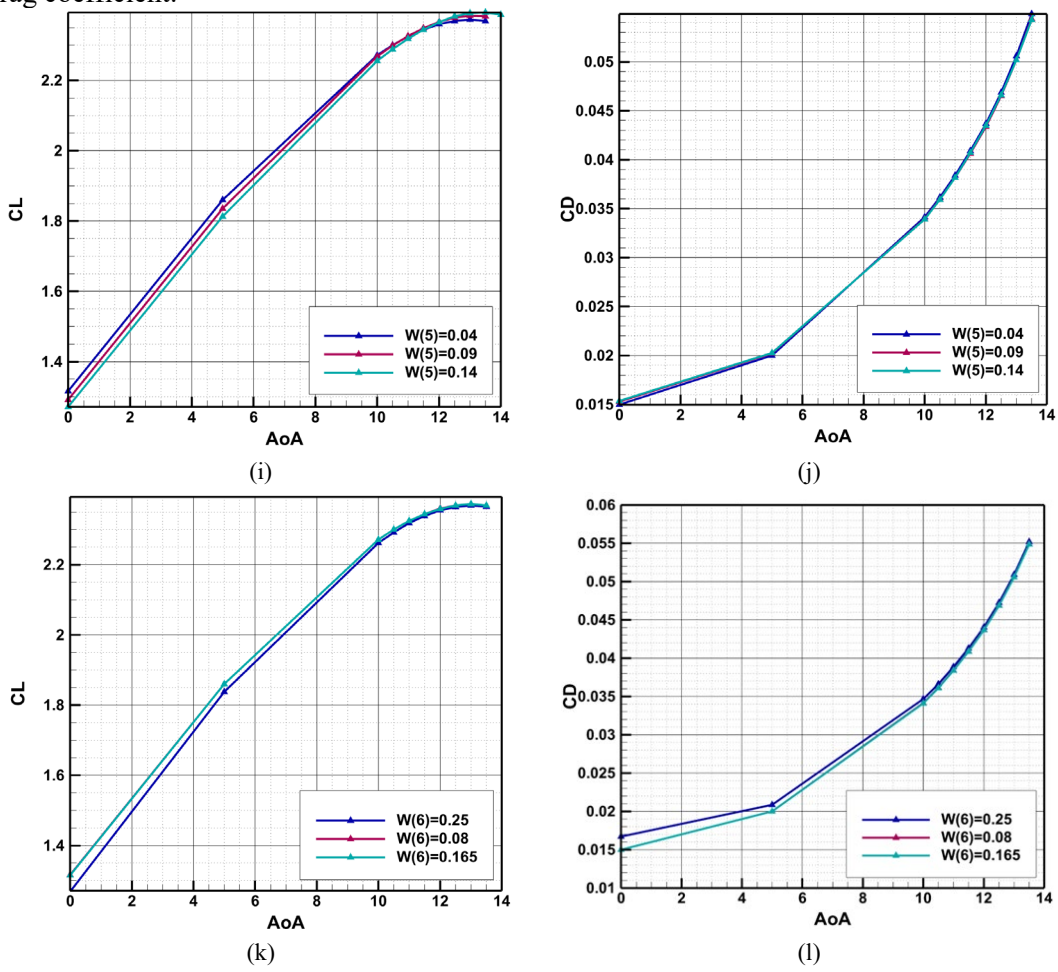

Fig. 15 $CL\ vs\ AoA$ and $CD\ vs\ AoA$ for different values of W_5(a-b) and W_6 (c-d)

The obtained results offer important insight in the assessment of the influence of flap geometry on aerodynamic characteristics. Certain parameters, such as the curvature radii of the internal geometry, as well as the aspect of the flap leading edge, affect the lift and drag coefficients only in the linear region, where parasitic drag has a more prominent impact than at higher angles of attack, where the influence of induced drag and flow separations becomes more noticeable. Parameters exhibiting the most significant variations are the ones determining the lip length and upper surface camber, where lower values are associated with higher lift coefficients and reduced drag, due to a larger flow exit area being created between the lip and flap.

C. Optimization Results

The optimization process has resulted in a modified configuration, whose geometry is presented in Fig. 16, defined by a substantially shorter lip, as well as a flat upper surface and a thinner leading edge. The obtained shape is validated by the parametric study, where results showed significant improvement in lift coefficient near stall for reduced lip length and upper surface flap camber.

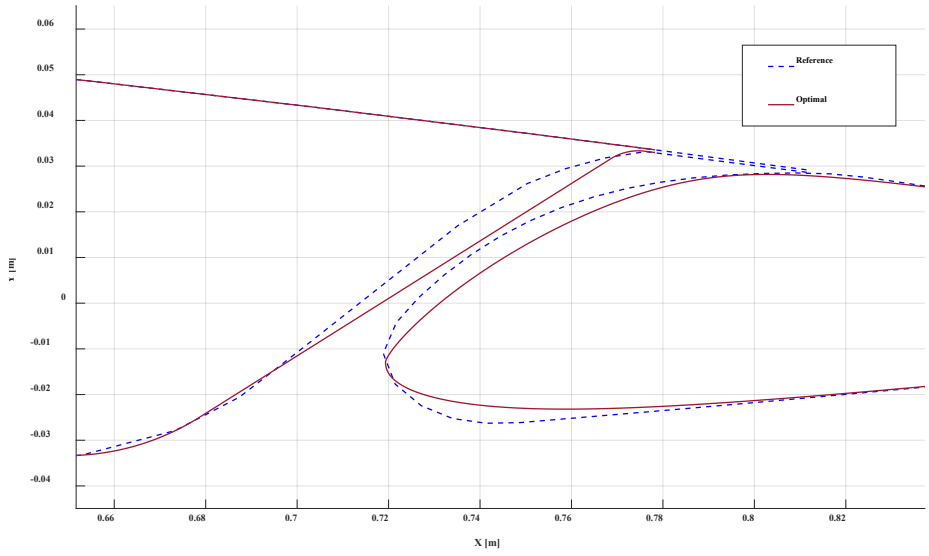

Fig. 16 The optimal geometry

During the optimization, the algorithm successfully identified the steepest gradient descent direction, therefore guiding the decision variables to improved values of the objective function. The convergence histogram in Fig. 17 shows a rapid decrease of the objective function within the first five iterations, followed by a plateau reached by iteration.

From iteration 10 onward, the solution stabilizes, and the objective function exhibits negligible variations, confirming that the optimization has effectively converged toward an optimal configuration.

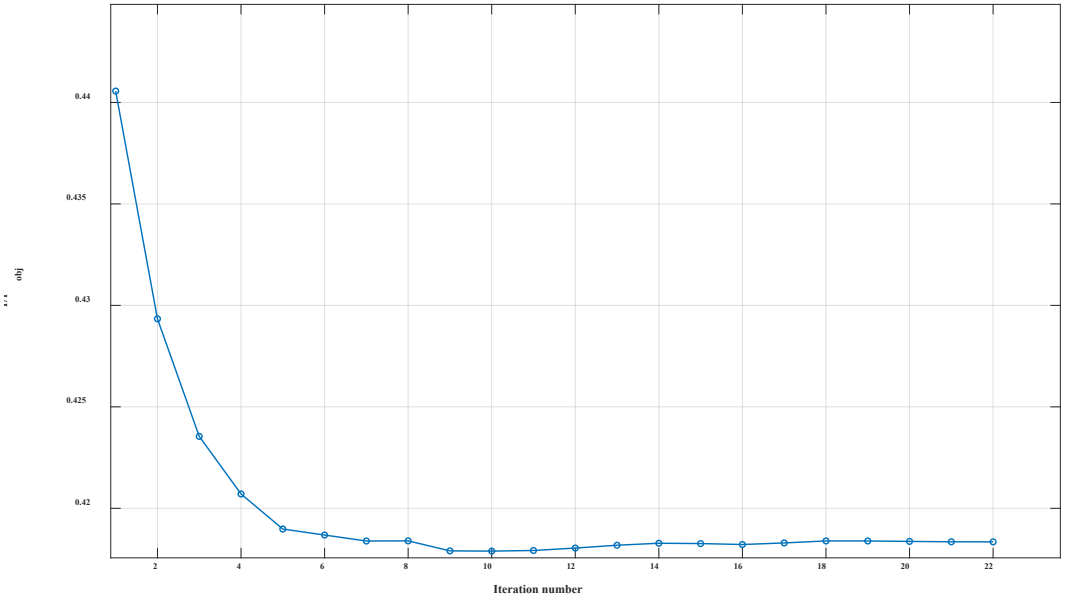

Fig. 17 Optimization convergence plot

The optimal configuration exhibits superior aerodynamic characteristics as compared to the baseline geometry in the stall region. Fig. 18 shows a 3.6% lift enhancement, alongside a 2% drag reduction at an angle of attack equal to 11.5°.

Although the obtained geometry does not surpass the reference at low angles of attack, the optimization is considered successful, since the objective function focused solely on the nonlinear, near-stall region. The CL/CD value of the optimised geometry is higher than the reference value for all angles of attack higher than 6°, with a maximum improvement of 8%, obtained at 11.5°.

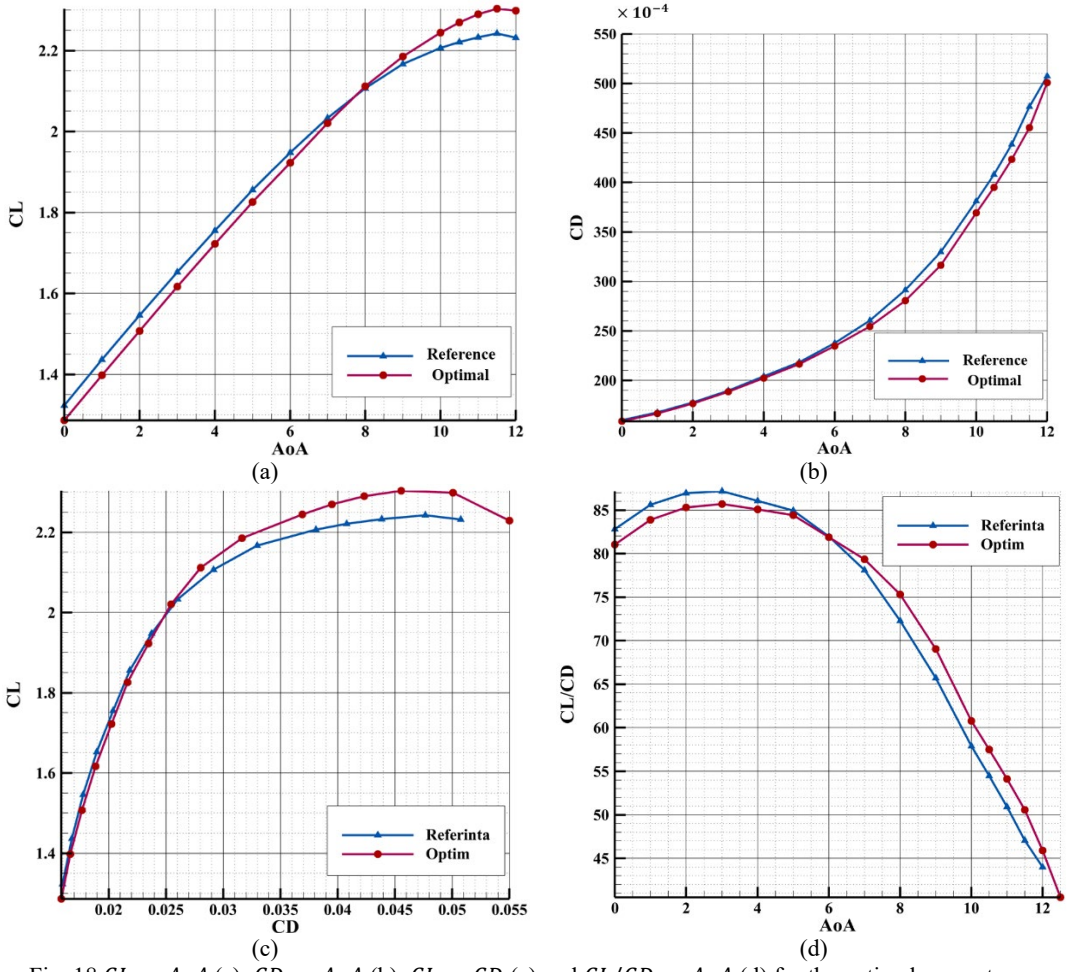

Fig. 18 $CL\ vs\ AoA$ (a), $CD\ vs\ AoA$ (b), $CL\ vs\ CD$ (c) and $CL/CD\ vs\ AoA$ (d) for the optimal geometry, as compared to the baseline

Fig. 19 presents the velocity contours and streamlines in the vicinity of the flap slot at zero angle of attack. The overall flow field highlights the acceleration of the jet through the slot, which energizes the boundary layer on the flap surface.

The velocity distribution suggests a strong acceleration on the flap, with maximum velocities higher than on the main airfoil, exceeding 120 m/s at the slot exit.

This phenomenon is more pronounced due to the narrowing section between the flap and the airfoil, the highly energized flow favorizing higher velocity magnitudes and attached flows downstream the flap.

Nevertheless, a recirculation region is visible on the airfoil, along with low velocity magnitudes around the lip.

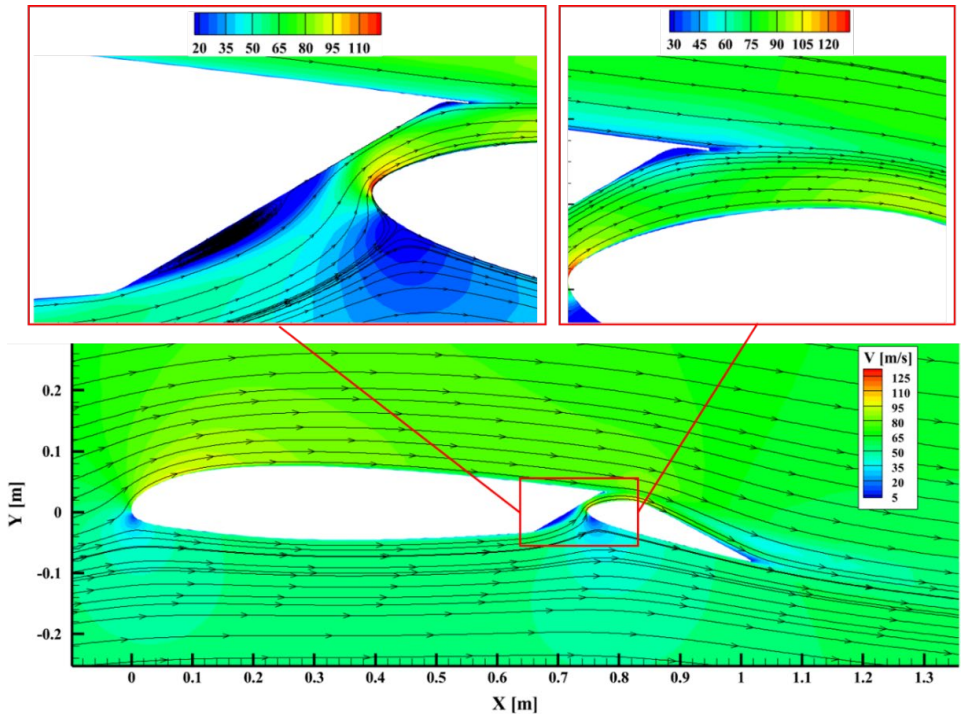

Fig. 19 Velocity contours and streamlines distribution for the optimal configuration at an angle of attack of 0°

As the angle of attack increases, the surface velocities rise, amplifying the acceleration of the flow at the slot exit. Fig. 20 presents a comparative velocity distribution of the investigated region, for both the baseline and the optimized configuration. The drag-inducing separation zone present in the reference geometry has been completed eliminated by varying the orientation of the tangent and reducing the radii of the slot. Furthermore, higher velocity magnitudes on the optimized flap, a direct effect of the less cambered flap and narrowing exit section, generate increased lift and keep the flow attached in the downstream.

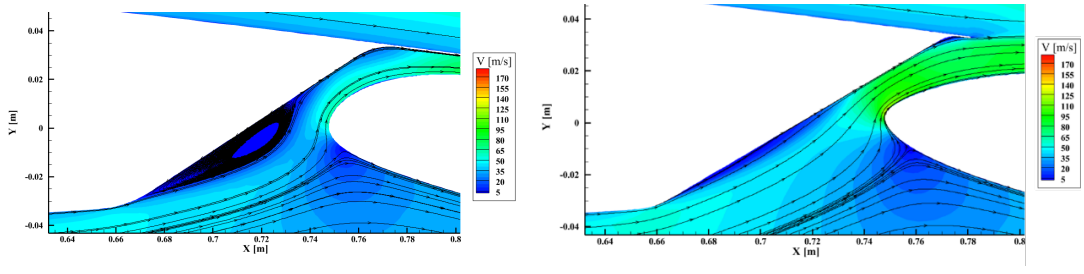

(a) Baseline configuration (d) Optimal configuration

Fig. 20 Comparative analysis of velocity contours around the baseline (a) and the optimal (c) configurations at $AoA = 11.5°$, corresponding to the stall angle of attack

4. CONCLUSIONS

This work has highlighted the critical role of flap slot geometry in shaping the aerodynamic characteristics of single-slotted high-lift configurations. By introducing a dedicated parametrization method based on cubic Bézier curves for the flap leading edge and local curvature radii for the internal channel, continuous and feasible geometries were generated

while preserving the constraints of the baseline retracted configuration. Then, by coupling the parametrization with a fully automated CFD workflow and gradient-based optimization framework, this methodology enabled a systematic exploration of the design space, significantly reducing time and effort while ensuring robust evaluation of hundreds of candidate geometries.

The parametric study, composed of 729 distinct configurations, revealed that the lip length of the flap channel and the curvature of the flap suction surface exert the strongest influence on aerodynamic characteristics at high angles of attack. Shorter lips were shown to energize the jet at the slot exit, enhancing boundary-layer attachment and suppressing flow separation, while favorable shaping of the inner surface improved lift generation. In contrast, the channel curvature radii had only a minor effect on lift but dictated the internal flow aspect, influencing the onset of recirculation and thereby affecting drag.

The optimization study confirmed the potential of precise geometric variations, obtaining configurations with up to 7% higher maximum lift and 5% lower drag compared to the baseline. These improvements are particularly relevant for low-speed regimes such as take-off and landing, where maximizing lift while controlling drag is essential.

ACKNOWLEDGMENT

The first author of this article was awarded The Ex aequo **"Nicolae TIPEI"** Prize Award: Bachelor-Master Category (awarded by the INCAS Scientific Council), at the "Awards Gala" of the *41st "Caius IACOB" Conference on Fluid Mechanics and its Technical Applications, held on 30 - 31 October, 2025*, at the headquarters of the INCAS, Blvd. Iuliu Maniu 220, sector 6, Bucharest, Romania.

REFERENCES

[1] * * * European Commission: Directorate-General for Research and Innovation and Directorate-General for Mobility and Transport, "Flightpath 2050 - Europe's vision for aviation - Maintaining global leadership and serving society's needs," Publications Office, 2011.

[2] P. Rouco, P. Orgeire-Crespo, G. D. R. Gonzalez and F. Aguardo-Agelet, "Airfoil Optimization and Analysis Using Global Sensitivity Analysis and Generative Design," *Aerospace,* vol. **180**, no. 12, 2025.

[3] T. Lin, R. Pecora, Ciliberti, Danilo, W. Xia and S. Hu, "Aerodynamic optimization of an adaptive flap for next-generation green aircraft," *Chinese Journal of Aeronautics,* vol. **37**, no. 2, pp. 100-122, 2023.

[4] A. Smith, "High-Lift Aerodynamics," *Journal of Aircraft,* 1975.

[5] J. Heinz, N. N. Sørensen and F. Zahle, "Investigation of the load reduction potential of two trailing edge flap controls using CFD," *Wind Energy,* vol. **14**, pp. 449-462, 2010.

[6] B. Steenwijk and P. Druetta, "Numerical Study of Turbulent Flows over a NACA 0012 Airfoil: Insights into Its Performance and the Addition of a Slotted Flap," *Applied Sciences MDPI,* vol. **13**, 2023.

[7] * * * NASA Langley Research Center, "Wind Tunnel Tests of the GA(W)-2 Airfoil with 20% Aileron, 25% Slotted Flap,30% Fowler Flap, and 10% Slot-Lip Spoiler," National Technical Information Service, Wichita, Kansas, 1976.

[8] J. Bodart, J. Larsson and P. Moin, "Large eddy simulation of high-lift devices," in *21st AIAA Computational Fluid Dynamics Conference*, San Diego, CA, 2013.

[9] B. M. Kulfan, "Universal parametric geometry representation method," *Journal of Aircraft,* vol. **45**, no. 1, pp. 142-158, 2008.

[10] H. Sobieczky, "Parametric Airfoils and Wings," *Notes on Numerical Fluids,* vol. **68**, pp. 71-88, 1998.

[11] G. Howe, "Optimization of 2-D Flap Geometry Using Matlab and," in *49th AIAA Aerospace Sciences Meeting including the New Horizons Forum and Aerospace Exposition*, Orlando, FL, 2011.

[12] S. Xiang, Q. Wen, M. Wei and Z. Jia, "Optimization of the double-slot blown airfoil with jet at the," *AIP Advances,* vol. **14**, 2024.

[13] Y. Yin and Y. Zhang, "Optimization and Analysis of a Blown Flap Based on a Multielement Airfoil," *Journal of Aicraft,* vol. **57**, no. 1, pp. 1-14, 2019.

[14] W. Chen, K. Chiu and M. D. Fuge, "Airfoil Design Parameterization and Optimization Using Bézier Generative Adversarial Networks," *Journal of Aicraft,* vol. **58**, no. 11, 2020.

[15] * * * National Advisory Committee for Aeronautics, "Wind Tunnel Investigation of an NACA23012 Airfoil with Various Arrangements of Slotted Flaps, Report No. 664," 1939.